Memoirs of the College of Science, University of Kyoto, Series A,
Vol. XXIX, No. 3, Article 4, 1961.

DROP PRODUCTION BY BURSTING OF AIR BUBBLES ON THE SEA SURFACE (III) STUDY BY USE OF A WIND FLUME

BY

Yoshiaki TOBA

(Received December 27, 1960)

ABSTRACT

Experiments on the air entrainment in wind waves and the drop production from them, are carried out by use of a wind flume, 21 m long. A new mechanism of the air entrainment, that is caused by instability of small waves which override gravity waves and in which the surface tension exerts to a considerable degree, is first observed. The lowest wind speed for the occurrence of this process is about 13 $m \cdot sec^{-1}$ (at 10 m level), which is considered to be one of the important critical wind speeds for air-sea boundary processes. Small droplets measured in the air above wind waves are confirmed to be produced by bursting of the air bubbles entrained in wind waves. Concentration-size distribution of the droplets in the air directly above the sea surface and density-mass distribution of sea-salt nuclei at various heights, are derived, by theoretical treatment, from the results of the experiment. After some modification, the latter nearly represents the actual distribution of giant sea-salt nuclei in the atmosphere. The rate of production of droplets of each size grade, estimated by the experiment, is ensured also by comparison with an observation of salt fallout near the coast. Dependence of the rate on wind speed also agrees with the field observation. Distribution of the entrained air bubbles in wind waves is measured, and the coefficient of mixing in wind waves is estimated from it.

1. Introduction

Part of the atmospheric condensation nuclei, especially giant salt nuclei which grow to droplets that can initiate rain from warm clouds, are believed to originate from the ocean surface. Further, it is presumed that sea water droplets which become salt nuclei are not large splashing water from wave crests, but are small droplets produced when air bubbles burst at the sea surface. Studies on the drop formation, by bursting of each bubble at sea water surface, has been made by several investigators (**1**, **2**, **3**, **4**, **5**, **6**, **7**, **8**, **9**). These investigations show that smaller bubbles eject droplets, having diameters of ten and odd percents of original bubbles, through disintegration of water jet formed upon collapse of a bubble cavity, and also that bubbles larger than a few mm produce comparatively many droplets of a few tens micron, through shuttering of the bubble film.

However, as to the actual process of entrainment of air bubbles in sea water and the drop formation from them, few studies have been made so far. Merely, D. J. Moore and B. J. Mason (5) caught droplets in the air flow above sea water in a wind-wave tunnel 6 m long; and D. C. Blanchard and A. H. Woodcock (7) measured the size and rate of rise of small bubbles in sea water, at the surf zone after a breaking surf passed and large bubbles rose to the water surface, and estimated the rate of formation of droplets through disintegration of jets from the bubbles.

In order to know the rate of supply of sea-salt nuclei into the upper air, it is first necessary to know the rate of production of sea water droplets at the air-sea boundary, or the distribution of the droplets in the atmosphere very near the boundary. Especially, quantitative as well as qualitative research of such dramatic phenomena like the entrainment of air bubbles in wind waves and droplet production from them, must be also in themselves part of the most important problems in the air-sea boundary processes. So a comprehensive experiment on the problem has been carried out, by use of a wind flume of a comparatively large scale, and a series of theoretical considerations has been made in connection with the actual distribution of sea-salt nuclei in the atmosphere, as well as with the salt fallout near the coast.

In the experiment, tap water was used, instead of sea water, to protect the installations from damage. There might be, in consequence, some discrepancy between the results and the real phenomena at the air-sea boundary. But, so far as the essentials of the physical processes are concerned, serious deviations would not be found in the results.

2. Procedure and condition of experiment

2.1. Procedure of experiment

The wind flume used is set up at Ujigawa Hydraulics Laboratory of Disaster Prevention Research Institute, Kyoto University. The flume part is 21.6 m long, 0.75 m wide, 1.02 m high, containing fresh water 0.5 m deep, the side walls being made of polished glass. The wind is uniformly rectified through wind tunnel 8.6 m long and wind speed at the entrance to the flume varies from 0.5 up to 12.1 $m \cdot sec^{-1}$. Reflection of waves is prevented by a gentle bottom slope at the end of the flume, while an effort is made to remove surface contamination by draining the surface water over the bottom slope at the end of the flume.

Room temperature was between 10°C and 19°C, while water temperature was between 10°C and 18°C, humidity having been between 86 percent and 57 percent, in the course of the present experiment.

Methods of measurement of various elements were as follows.

(i) *Distribution of wind speed*

Wind speed profiles were measured by use of a miniature anemometer of Robinson type, up to the height of 35 cm above the undisturbed water surface, at 4.5 m, 6.9 m, 10.0 m and 13.6 m in fetch. The mean wind speed in the cross section of the wind tunnel was also measured at the entrance to the flume.

(ii) *Elements of wind waves*

Wave form was registered by an ink-writing oscillograph connected with a resistance type wave-meter of H. Kunishi (**10**), at the above-mentioned four fetches. Period and height of waves were read on the records, and the wave length was calculated from the wave period, by the well-known formula for surface waves, in which the surface tension is also taken into account.

(iii) *Bubbles*

The room was darkened and bubbles were photographed under an illumination. A camera was set at a fixed distance of 1 m or 60 cm from the glass wall, and the focus was arranged at 3 cm inside the wall. The depth of the focus was 3.5 cm or 1.3 cm, respectively. Bubbles on photographs were read, by use of a moving microscope with an arranged scale. Bubbles in water were not round but flat, so that vertical and horizontal diameters were read for each bubble and converted into an equivalent diameter, by assuming the bubble shape to be an ellipsoid. Motion pictures (64 frames per sec) and stereographs of bubbles entrained in wind waves, were also taken at a fetch of 10 m.

(iv) *Droplets*

Droplets larger than 100μ were caught by a dye-treated filter paper 2 cm wide, held vertical and normal to the wind. Method of the measurement is referred to Y. Toba (**11**). For smaller droplets, a glass slide 5 mm wide coated with MgO (**12, 13, 14**) was adopted. The ratio 0.86, between the droplet diameter and the diameter of the crater made by it, was used. For droplets of 150~250μ and 250~350μ, both methods gave equivalent results, while for droplets of 100~150μ, results by filter paper seemed to be unreliable, so that only results by glass slides were adopted for this size. The efficiency of drop deposition on the filter paper and glass slides, was checked by I. Langmuir and K. B. Blodgett's method (1945) cited in A. H. Woodcock and M. M. Gifford (**15**), and the measured number of droplets for each diameter grade was multiplied by a correction factor. This factor was found to be significant only for droplets smaller than 50μ. Observation of droplets was also made at the same fetches together with observation of wind profiles, at the height ranging from 8 cm to 25 cm, where wind profiles obey the logarithmic law.

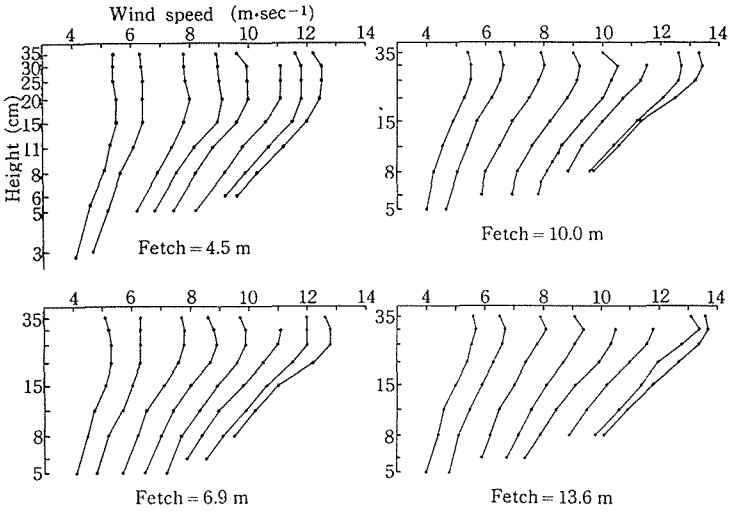

Fig. 1. Distribution of the wind speed. Heights are measured above the still water surface.

Table 1. The mean wind speed in the cross section of the wind tunnel and the wind speed at 10 m level.

Mean wind speed (m·sec⁻¹)	12.1	11.6	10.8	9.7	8.7	7.5	6.1	5.1
Wind speed at 10 m level (m·sec⁻¹)	22.8	21.4	18.7	16.5	14.9	12.6	10.3	8.7

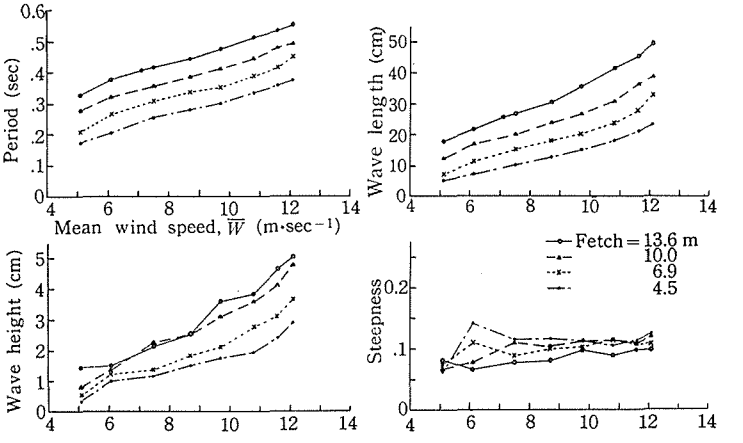

Fig. 2. Elements of the main wind waves.

2.2. Distribution of wind speed and elements of wind waves

Eight grades of the mean wind speed, ranging between 5.1 m·sec^{-1} and 12.1 m·sec^{-1}, were used. The observed wind profiles at each fetch are illustrated in Fig. 1. Retween 8 cm and 15~25 cm in height, they were represented approximately by the logarithmic law. Wind speeds at 10 m level were calculated by extrapolating these values. The values are listed in Table 1.

Average period and average wave height of the main gravity waves read from the wave records, and wavelength and steepness calculated from them are illustrated in Fig. 2.

3. Air entrainment in wind waves

3.1. Mechanism of the air entrainment in wind waves

The breaking of crests of large gravity waves reached to a maximum steepness has been so far regarded as the principal mechanism of the air entrainment and bubble formation in wind waves. At shores, a plunging breaker is considered to be an effective mechanism for the entrainment of bubbles. In the present experiment, another important mechanism has been observed for the first time. It is the entrainment of air bubbles caused by instability of small waves which override the large gravity waves, and in which the surface tension exerts to a considerable degree.

W. H. Munk (**16**) proposed a hypothesis for the fact that short wavelets are found forward of the crests of large waves. According to him, it is in such conditions that the sum of the phase velocity of foregoing capillaries and the orbital velocity of underlying wave is equal to the phase velocity of the underlying wave. A. H. Schooley (**17**) observed, in a small wind-wave tunnel, capillary waves which ride on the front of larger gravity waves and progressed with the same velocity as that of larger gravity waves. In the present experiment, these fine capillaries are also observed for 5 or 6 m·sec^{-1} in the mean wind speed (Fig. 3). But when the interference between trains of underlying gravity waves affects the orbital velocity of the waves, this condition breaks, and capillary waves that exist closest to the crests, are observed to move back relatively to the main gravity waves, and again lead the next crests of gravity waves.

When the wind speed increases further and main gravity waves become larger and more irregular, the above regularity no longer exists and all over the water surface becomes covered by wavelets, the wavelength of which is less than several cm, and which progress backward relatively to the main gravity waves. Fig. 4 shows this stage. At the first glance, main gravity wave train progresses with

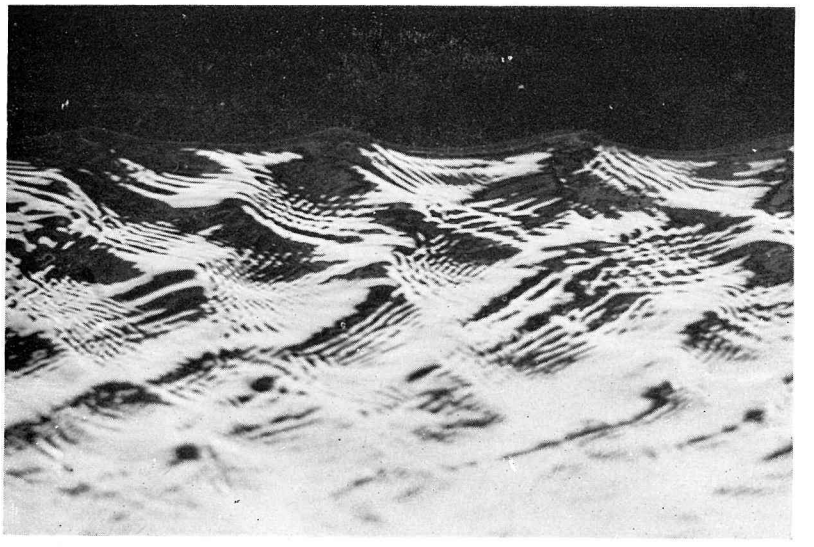

Fig. 3. Water surface seen from beneath. Capillary wave crests intersect one another. ($\overline{W}$=6.1 m·sec^{-1}, Fetch=4.5 m)
The width of all the photographs is about 35 cm.

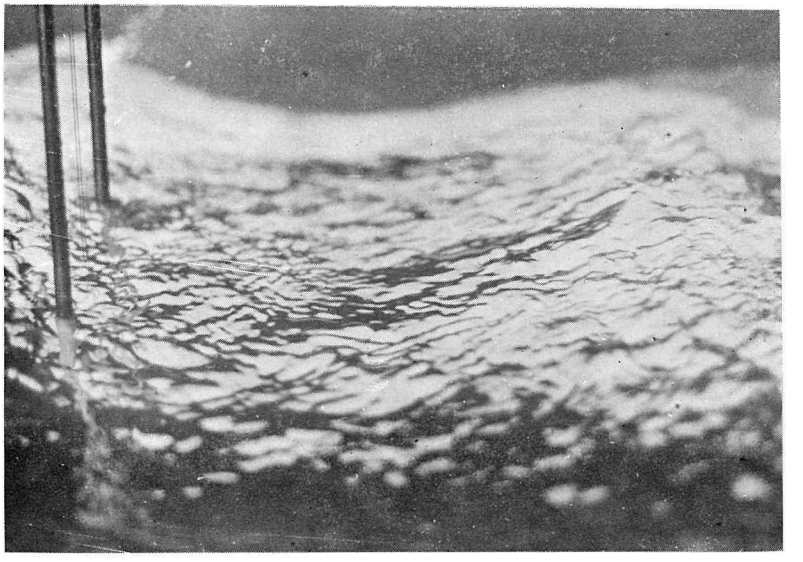

Fig. 4. Roughness rides all over the main wave train. ($\overline{W}$=11.6 m·sec^{-1}, Fetch=6.9 m)

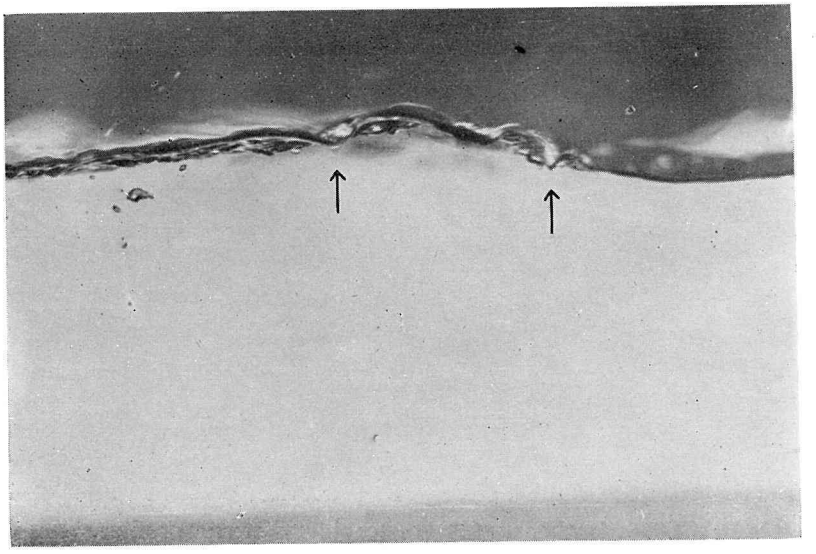

Fig. 5. Profiles of wavelets, which peak downwards. ($\overline{W}$=8.7 m·sec^{-1}, Fetch=13.6 m)

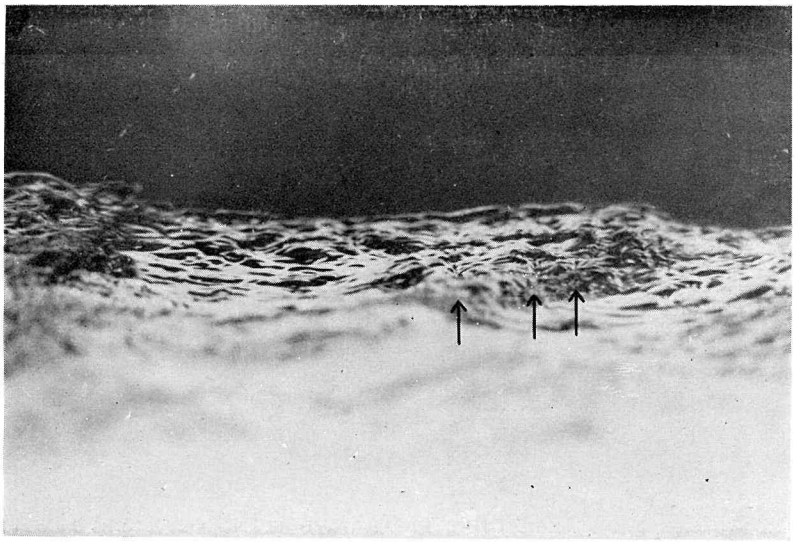

Fig. 6. Roughness from beneath. It looks like a ceiling of a stalactite grotto. ($\overline{W}$=11.6 m·sec^{-1}, Fetch=4.5 m)

a certain speed, and wavelets on it exist at random. However, if one turns one's eyes away from the main wave train, and set them to wavelets, one will find a pattern of wavelets progressing with a speed smaller than that of the gravity wave train which passes through it. It appears to converge where crests of main waves pass, and diverge where troughs of them pass, namely, it seems that, through a medium of the pattern of wavelets, a longitudinal wave train progresses with a phase velocity equal to that of the main gravity wave train. This kind of convergence had been pointed out by P. J. H. Unna (**18**) for larger gravity waves, and was cited by Munk (**19**). This kind of convergence and the interference of wavelets, as shown in Fig. 3, increase the steepness of the wavelets. These wavelets of large steepness also have a profile that peaks downwards, which is the reverse of the case of gravity waves, as Schooley (**17**) observed for small capillary waves. Fig. 5 shows the typical profile of this type. The water surface, as seen from beneath, looks like a ceiling of a stalactite grotto (Fig. 6). This again confirms G. D. Crapper's theory (**20**) of capillary wave profiles. As Crapper suggested for pure capillary waves, air bubbles are enclosed at the troughs, and scatter into water by turbulence as shown in Fig. 7. Since the profile of these wavelets may be determined by factors such as the surface tension, the acceleration of gravity, the viscosity, etc., bubbles thus entrained will have a definite size range, but because of the very complicated situation the definite size range does not manifest itself apparently. Further developed conditions of the air entrainment of this type are shown in Fig. 8. Although bubbles are being entrained, basic gravity wave itself is not always breaking, as understood from the photograph.

The condition in which this mechanism of the air entrainment first occurs will be shown in **3.3.** The wind speed is much greater than force 4 on the Beaufort scale, and is about $13\,\mathrm{m\cdot sec^{-1}}$ (10 m level). This mechanism is expected to occur all over the crests of comparatively small gravity waves at the sea surface, when wind speed exceeds further this value. This wind speed is considered to be an important critical wind speed for air-sea boundary processes. As this mechanism of the air entrainment is much affected by the surface tension of sea water, a change in the surface tension at the sea surface may result in a corresponding change in the rate of production of sea-salt nuclei over the oceans.

3.2. Distribution of the air bubbles in wind waves

Bubbles are entrained when some main wave crests pass, and rise through water until the next entrainment occurs. To obtain an average vertical distribution of entrained bubbles, for each wind speed and for each fetch, it is desirable to take at random time a number of photographs for each condition, and to take an

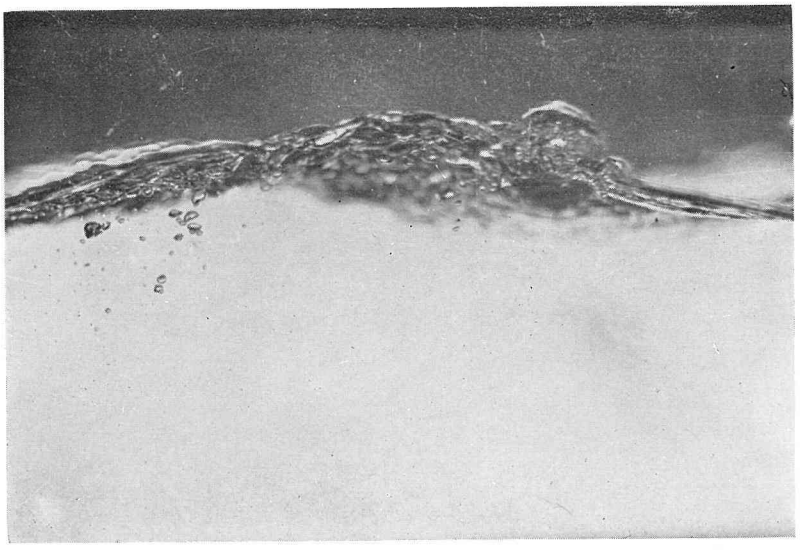

Fig. 7. Bubbles are being entrained in wind waves. ($\overline{W}$=10.8 m·sec^{-1}, Fetch=13.6 m)

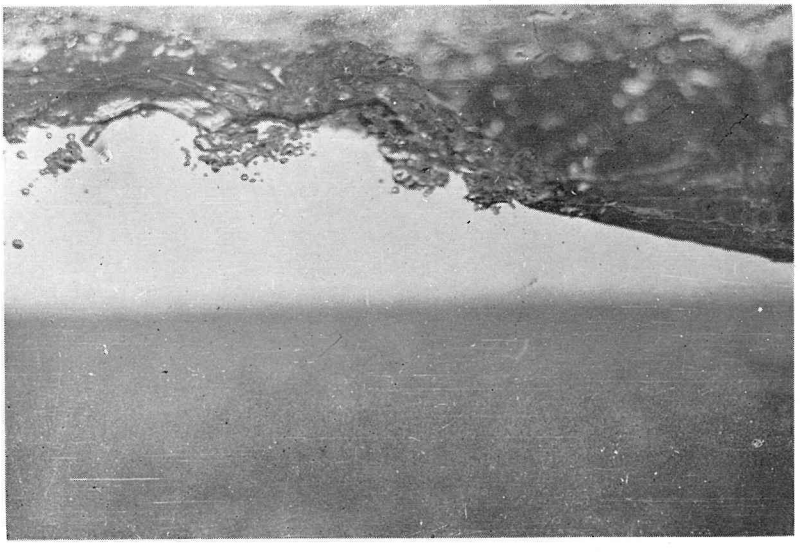

Fig. 8. Further developed conditions of the air entrainment. ($\overline{W}$=11.6 m·sec^{-1}, Fetch=13.6 m)

average of them. But it is rather useless, because there appears no bubble on the majority of the photographs, especially for lower wind speeds. Thus, an alternative method is employed to take rather a small number of photographs, by aiming at instances when bubbles come in sight of the camera, and to estimate the average distribution of bubbles by use of the other properties together, which are explained in the next section.

The number and the size of bubbles on photographs have been read for each depth below the water surface. Examples of the vertical distribution of bubble number are shown in Fig. 9. As seen in the figure, the number of bubbles decreases exponentially with increasing depth. This vertical distribution can be used to estimate the coefficient of mixing in wind waves, which will be mentioned in the last section of this paper.

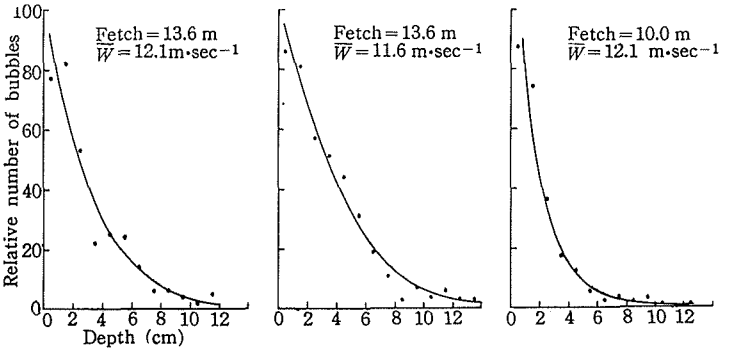

Fig. 9. Examples of the vertical distribution of the entrained air bubbles in wind waves.

3. 3. Rate of entrainment of the air bubbles in wind waves

It can be considered that there exists an equilibrium condition, in an average, between bubbles entering from water surface and those rising to the surface. Consequently, the average rate of entrainment of bubbles (B) can be estimated by the product of average concentration at the surface (θ_0) and the rising velocity (w) of bubbles for each bubble size. Namely,

$$B = w\theta_0 .$$

But, θ_0 is not known and what is actually known is θ_0', which is an average surface concentration of bubbles at a region of the wave train where bubbles are formed. To reduce θ_0' to θ_0, some factors that represent a proportion of the region of wave train where bubbles exist to that where they do not, must be multiplied. One factor is $\alpha/100$, where α represents the percentage of crests

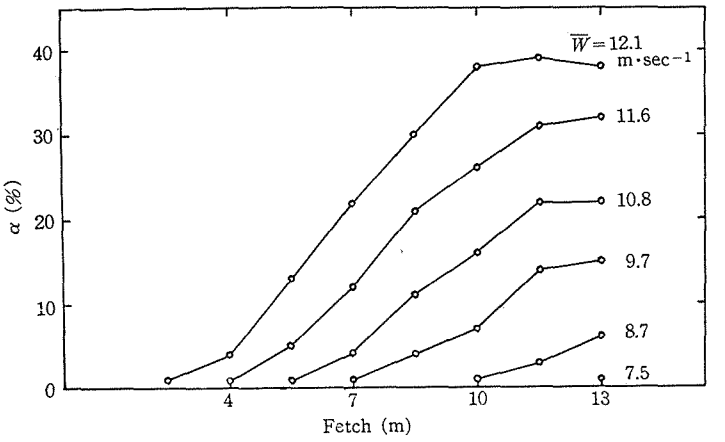

Fig. 10. Values of α: the percentage of crests of main gravity waves that are entraining air bubbles.

of main gravity waves that are entraining air bubbles (not all of the crests of main gravity waves entrain bubbles). Values of α are shown in Fig. 10.

As seen from the figure, the lowest wind speed for the occurrence of the air entrainment at 13 m in fetch, is 7.5 m·sec^{-1} in the mean taken in the tunnel section, and this corresponds to 13 m·sec^{-1} at 10 m level. The critical wind speed increases with decreasing fetch. However, curves in Fig. 10 seem to saturate already at 13 m in fetch, so that this critical wind speed may apply to the open ocean.

The other factor is $[\theta']/Tw\theta_0'$, where $[\theta']$ means the total number of bubbles, for each size grade, contained in a water column of unit base area, and T is the period of the main wave. The ratio $[\theta']/w\theta_0'$ means a sort of residence time, or an average life-time of bubbles in water. The terminal velocity of the air bubbles in water (w) was examined critically in a paper by R. L. Datta *et al.* (**21**). According to it, the velocity of small bubbles increases almost linearly with an increasing bubble size, and reaches about 32 cm·sec^{-1} for a bubble of 2 mm in diameter, then decreases to 24 cm·sec^{-1} for one of about 6 mm, and then increases slowly. The residence time is generally smaller than T. The ratio of the residence time to T is thus understood to be necessary for reducing θ' to θ. Consequently, B is given by

$$B = w\theta_0' \times \frac{\alpha}{100} \times \frac{[\theta']}{Tw\theta_0'}$$

$$= \frac{\alpha}{100T}[\theta'] .$$

The calculated value of B for each fetch and each wind speed is illustrated

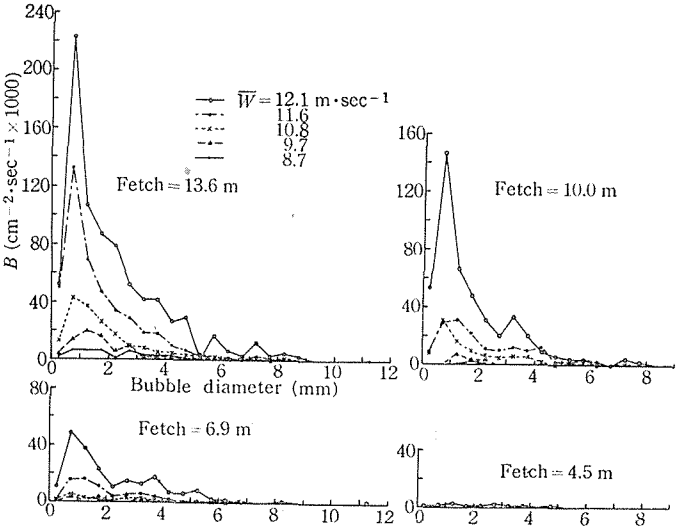

Fig. 11. Values of B: the rate of formation of air bubbles in wind waves.

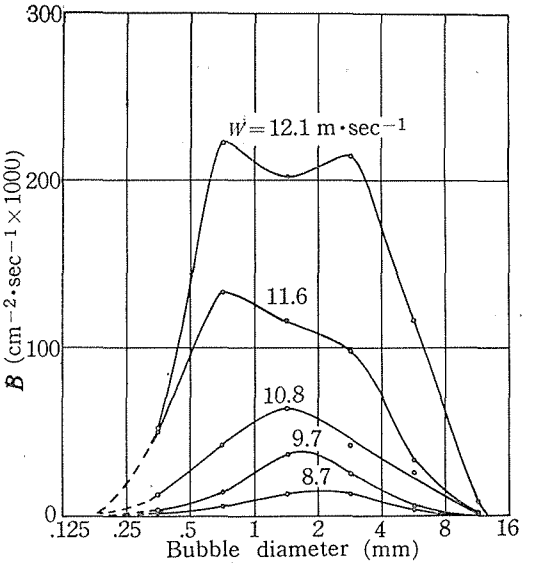

Fig. 12. Values of B per equal log(bubble size) interval, for 13.6 m in fetch.

in Fig. 11 for each bubble size. From this figure it is found that bubbles between 0.5 mm and 1 mm in diameter are observed most frequently, and that this dominant peak diminishes rapidly as the wind speed decreases or as the fetch decreases, namely, as the rate of bubble entrainment decreases. Bubbles of this peak seem to be produced by great disturbance of water due to turbulent motion in waves, when bubbles are being entrained. The values of B per equal log(bubble size) interval, are calculated by smoothed values from Fig. 11, and are shown in Fig. 12 for 13.6 m in fetch. The curves have nearly symmetrical shapes, with their axes between 1 mm and 2 mm in bubble diameter, the axes tending to shift to larger diameters for lower wind speeds.

4. Drop production from wind waves

4.1. Drop production by bursting of air bubbles

It seems that there are at least two different mechanisms of drop production by bursting bubbles. One is the disintegration of water jet formed upon collapse of a bubble cavity. Relations among the size, the number and the height of the ejection of these droplets, and the bubble size and the temperature for sea water were studied by C. G. Boyce (**1**), D. C. Blanchard and A. H. Woodcock (**7**), S. Hayami and Y. Toba (**8**) and others (**2**, **3**, **4**, **5**, **6**, **9**), and for fresh water, by O. Stuhlman Jr. (**22**) and D. M. Newitt *et al.* (**23**). From these results, one can see that the droplets have a size of ten and odd percents of the original bubbles, and that the occurrence of this mechanism is mainly restricted to bubbles smaller than 4 mm in diameter, and further that the ejection is most conspicuous for droplets of about 300μ in diameter.

The other mechanism seems to concern with the shuttering of bubble film. Using sea water, B. J. Mason (**6**) observed that, besides the large drops produced by disintegration of the jets, bubbles greater than 2 mm diameter produced a second group of droplets having diameters between 5μ and 30μ, bubble of 2 mm diameter producing, on an average, only about one droplet in this size range. This group of droplets was also measured by D. M. Newitt *et al.* (**23**), who measured for bubbles ranging between 3.1 mm and 5.3 mm of fresh water. The mean size of these droplets lay between 60μ and 20μ. The majority of these droplets were formed below 1 cm in height. The number of these droplets is found to be nearly proportional to the area of bubble film calculated by Y. Toba (**24**), and about 50 per 1 cm^2 of the film, as shown in Table 2. This relation seems to show that this group of droplets is produced by shuttering of bubble film. Experiments by K. Isono (**9**) on bubbles of sea water of 3 mm diameter also show similar results in size distribution of droplets, but the number is rather large.

Table 2. Summarized relation between bubbles and droplets produced from them.

Bubble diameter (mm)	Droplets from jet: Allotment of bubble number (%)	Droplets from jet: Diameter (μ)	Droplets from jet: Number per bubble	Droplets from film: Number assumed to be 50 per 1 cm² of bubble film (Diameter: 0~50μ)	Droplets from film: Number from data by Newitt *et al.* (23)
0 ~ 0.5		0~ 50	4		
0.5~ 1.0	80	50~100	4	0.005	
	20	100~150	4		
1.0~ 1.5	40			0.045	
	60	150~250	3.6		
1.5~ 2.0	46			0.17	
	54	250~350	2.5		
2.0~ 2.5	46			0.42	
	54	350~450	1.6		
2.5~ 3.0	32			0.90	
	68	450~550	1		
3.0~ 3.5	20			1.6	1.6
	80	550~650	1		
3.5~ 4.0	10			2.7	2.4
	90	650~750	1		
4.0~ 4.5				4.3	3.8
4.5~ 5.0				6.2	6.0
5.0~ 5.5				8.7	11
5.5~ 6.0				11.6	
6.0~ 6.5				15	
6.5~ 7.0				19	
7.0~ 7.5				23	
7.5~ 8.0				29	
8.0~ 8.5				35	
8.5~ 9.0				42	
9.0~ 9.5				50	
9.5~10.0				58	

Table 3. Values of F_1': the rate of droplet production from wind waves, estimated from the rate of entrainment of bubbles, at 13.6 m in fetch. ($cm^{-2} \cdot sec^{-1} \times 10^3$)

Droplet diameter (μ)		$\overline{W}$ (m·sec^{-1}) 12.1	11.6	10.8	9.7	8.7
0~ 50	From jet	210	200	59	16	6.8
	From film	1700	450	220	66	37
	Sum	1900	650	270	82	44
50~100		710	420	140	45	18
100~150		400	220	92	43	16
150~250		390	230	122	71	24
250~350		200	100	58	35	14
350~450		91	45	22	13	6.1
450~550		48	22	9.0	5.3	2.9
550~650		42	19	6.5	3.7	2.4
650~750		34	13	5.0	2.8	1.8

Mason (6) found, in a cloud chamber, that bursting bubbles produced much larger numbers of particles of a third group too small to be detected by conventional methods. The number of these particles was between 100 and 200 for a bubble of 3 mm diameter, and their salt contents lay between 10^{-15} gm and 2×10^{-14} gm ($0.4\sim1.0\mu$ in droplet diameter). Droplets of this group were far small to produce giant nuclei.

Difference between sea water and fresh water may be significant, but it does not seem to be essential, at least so far as the results of the above-mentioned experiments of drop production reveal. For example, the efficiency and a critical point of drop ejection, measured by Hayami and Toba (8) by sea water bubble, seem indistinct in the experiment by Newitt *et al.* (23) for fresh water, but the latter shows similar features to the former; namely, the efficiency of drop ejection by jet disintegration seems to fall from about 3 mm to zero by about 6 mm diameter. The size of ejected droplets is also close in both cases.

Relations which combine the rate of bubble formation with the rate of droplet formation from the bubble, are summarized in Table 2, which also contains the comparison between the number of droplets produced by shuttering of bubble film obtained by assuming the production rate to be 50 per 1 cm^2 of film, and the value from the experiment by Newitt *et al.* (23).

4.2. Rate of drop production estimated from the entrained air bubbles in wind waves

Using Table 2 and smoothed values of B in **3.3**, the rate of drop production from wind waves is estimated as shown in Table 3 for 13.6 m in fetch. It is seen that the number of droplets produced by film shuttering is much larger than that by jet disintegration. The items of the former are illustrated in Fig. 13, showing that bubbles of several mm in diameter are most responsible for drop formation of this group.

4.3. Distribution of water droplets in space above wind waves

From the number of droplets caught, in a given time interval, by dye-treated filter paper and glass slides coated with MgO and from wind profiles, the number of droplets contained in a unit volume of the air was calculated for each drop size grade, by taking account of the drop deposition error on ribbons. The size grades smaller than 350μ are listed in columns I and II of Table 4. The typical examples of the distribution are shown in Fig. 14 for 13.6 m in fetch. Results of the droplet measurement by dye-treated filter paper, are also close to results of an experiment carried out by S. Okuda and S. Hayami (25) on the evaporation from wavy surface, by use of the same wind flume.

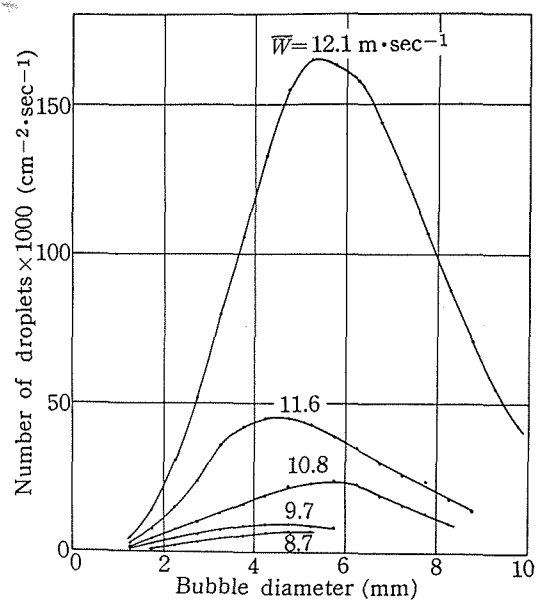

Fig. 13. Relation between the number of droplets produced by shuttering of bubble film and bubble diameter, for 13.6 m in fetch.

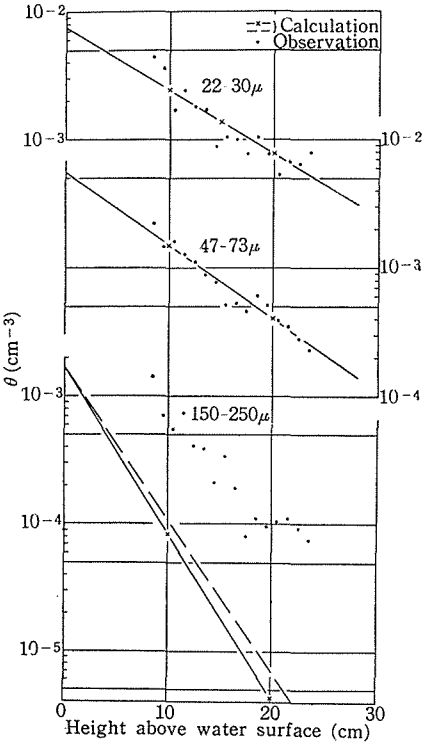

Fig. 14. Examples of the distribution of droplet concentration (θ) in the wind-flume, observed and calculated, for $\overline{W}$= 12.1 m·sec^{-1} and fetch=13.6 m. The broken line is the calculated curve by Eq. (4) below.

Consistency of the distribution of droplets in the space above wind waves, with the rate of production of droplets estimated in the last section, will be examined theoretically in the following chapter. The result will confirm that the droplets are produced by bursting of the entrained bubbles. However, much larger droplets that had diameters of 1 mm or more were caught occasionally. They could be distinguished from droplets produced by bubbles because of their extraordinary sizes. They are considered to be sprashing water from wave crests.

5. Theoretical considerations

5.1. Process of diffusion of droplets produced at the air-water boundary

Consider a simple case where wind blows uniformly in a horizontal direction. Take the coordinate origin at the entrance to the flume, the x-axis in the direction of the wind velocity, and the z-axis positive upward from the still water surface.

For the sake of convenience, consider a class of droplets of the same diameter, or of the same terminal velocity. Let u denote the wind velocity, w the terminal velocity of the droplet falling in the air, η the coefficient of mixing, and θ the number of droplets contained in the air per unit volume, or the concentration of droplets in the air. Then, the equation of droplet distribution in the air is given, under stationary conditions, by

$$u\frac{\partial\theta}{\partial x}=w\frac{\partial\theta}{\partial z}+\eta\frac{\partial^2\theta}{\partial z^2}. \tag{1}$$

Boundary conditions are

$$\left.\begin{aligned} -\eta\frac{\partial\theta}{\partial z}&=F(x) && \text{at}\quad z=0\ ,\\ \theta&=0 && \text{at}\quad z=\infty\ ,\\ \theta&=0 && \text{at}\quad x=0\ , \end{aligned}\right\} \tag{2}$$

and

where $F(x)$ represents the time rate of production of droplets per unit area of the water surface. The solution of Eq. (1) subject to the conditions (2) is given by

$$\theta=\int_0^x F(x-\lambda)\left\{\frac{1}{\sqrt{\pi\eta u\lambda}}\,e^{-\frac{1}{4\eta}\left(\frac{uz^2}{\lambda}+\frac{w^2\lambda}{u}+2wz\right)}-\frac{w}{2\eta u}\operatorname{erfc}\left(\frac{w\sqrt{\lambda}}{2\sqrt{\eta u}}+\frac{z\sqrt{u}}{2\sqrt{\eta\lambda}}\right)\right\}d\lambda, \tag{3}$$

where

$$\operatorname{erfc}(x)=1-\frac{2}{\sqrt{\pi}}\int_0^x e^{-t^2}dt.$$

For infinitely long fetch the solution becomes

$$\theta=\frac{F}{w}e^{-\frac{w}{\eta}z}=\theta_0 e^{-\frac{w}{\eta}z}. \tag{4}$$

In this case, F is considered as constant.

Further, when the droplet distribution given by Eq. (4) is brought on land where the production of droplets at the boundary does not exist any longer, the boundary conditions for Eq. (1) become

$$\left.\begin{aligned} \theta&=\frac{F}{w}e^{-\frac{w}{\eta}z} && \text{at}\quad x=0\ ,\\ \theta&=0 && \text{at}\quad z=\infty\ ,\\ \frac{\partial\theta}{\partial z}&=0 && \text{at}\quad z=0\ , \end{aligned}\right\} \tag{5}$$

and

where the origin of the x-axis is taken at the coast. The solution for this case is given as follows:

$$\theta = F\left[\frac{1}{w}e^{-\frac{w}{\eta}z} - \int_0^x \left\{\frac{1}{\sqrt{\pi\eta u x}}e^{-\frac{1}{4\eta}\left(\frac{uz^2}{x}+\frac{w^2x}{u}+2wz\right)} - \frac{w}{2\eta u}\operatorname{erfc}\left(\frac{w_1\sqrt{x}}{2_1\sqrt{\eta u}}+\frac{z_1\sqrt{u}}{2_1\sqrt{\eta x}}\right)\right\}dx\right]. \quad (6)$$

5.2. Comparison of theoretical calculations with data from the experiment —Determination of the rate of droplet production from wind waves

To calculate θ by Eq. (3), it is necessary to determine $F(x)$. In a range of the fetch within which the present experiment was carried out, F can approximately be expressed, as seen from the values in Fig. 11, by

$$F = F_1(x-x_0)/(1360-x_0)\ ,$$

where F_1 represents the value of F at 13.6 m in fetch, x_0 being the fetch where the air entrainment began to take place. For the case of $\overline{W}=12.1\ \mathrm{m\cdot sec^{-1}}$ ($\overline{W}$: the mean wind speed in the tunnel section), 460 cm was adopted for x_0.

The terminal velocity (w) of a water droplet smaller than about 1.7 mm in diameter can be calculated from knowledge of the fluid resistance exerting upon a moving sphere. Values of w has been calculated from the formulae by C. N. Davies (1945), which are expressed as follows (26):

$$Re = \frac{C_D Re^2}{24} - 2.3363\times10^{-4}(C_D Re^2)^2 + 2.0154\times10^{-6}(C_D Re^2)^3 - 6.9105\times10^{-9}(C_D Re^2)^4\ ,$$

$$\text{for } Re<4 \text{ or } C_D Re^2<140\ ;$$

$$\log Re = -1.29536 + 9.86\times10^{-1}\log(C_D Re^2) - 4.6677\times10^{-2}[\log(C_D Re^2)]^2 + 1.1235\times10^{-3}[\log(C_D Re^2)]^3\ ,$$

$$\text{for } 3<Re<10^4 \text{ or } 100<C_D Re^2<4.5\times10^7\ ,$$

where Re and C_D represent Reynolds number and drag coefficient, respectively. They are given by

$$C_D Re^2 = 4(\rho_l-\rho_a)gd^3/3\rho_a\nu^2\ ,$$

and

$$w = \frac{\nu Re}{d}\ ,$$

where d is the diameter of the sphere, ν is the kinematic viscosity of the air, and ρ_l and ρ_a are the density of the liquid and the air, respectively. It is noticed that the water drop of diameter 142μ represents a critical point in the law of terminal velocity. Droplets smaller than about this size (containing 7.5×10^{-8} gm of salts) can be picked up into the upper air easily as seen from the following section.

For the value of u, $1000\ \mathrm{cm\cdot sec^{-1}}$ (a value at about $z=10$ cm) has been used.

The value of η is said to be estimated by $\eta=0.4\,w_*z$, where w_* is the friction velocity. It has been evaluated from the data obtained by H. Kunishi (**27**) on the structure of wind stress, based on measurements of the distribution of wind velocity in the same wind flume. It is found that $w_*=107$ or $\eta=26.9z$ for $\overline{W}=12.1\,\mathrm{m\cdot sec^{-1}}$. Thus, it is presumed that the representative value of η in the present experiment is about 250 c.g.s. for $\overline{W}=12.1\,\mathrm{m\cdot sec^{-1}}$.

By Eq. (3) θ was calculated numerically for a case of droplets of 50~100μ in diameter, for $\eta=500$ and $\eta=250$, respectively. The values are shown in Fig. 15 by circles and crosses respectively. The distribution of θ calculated by assuming $\eta=250$ has the same gradient with the observation, but somewhat shifting upwards. This shift must result from an overestimation of F_1. The value of $\eta=250$ is applied to all the drop size grades and examples of the calculation are shown in Fig. 14 by crosses. For drop size smaller than 100μ, the calculation has been performed by taking at first F_1 to be unity, and parallel translation of the results has been made to fit the observations, the distance of translation representing the true value of F_1. Thus obtained values of F_1 are tabulated in column IV of Table 4. The corresponding values of F_1 estimated from the entrained bubbles and denoted as F_1' (Table 3), are shown in column V, and the ratio F_1/F_1' is shown in column VI. For droplets smaller than 100μ, the ratio is about 0.3. This discrepancy between F_1 and F_1' can be well understood by the fact that F_1' has been calculated by an assumption that each bubble produces droplets in a way shown in Table 2, but, in fact, flocking and coalescence of bubbles occur at the water surface and reduce the rate of formation of droplets. The reduction factor thus seems to be about 0.3 in the case of our experiment.

For droplets of 150~250μ, the observed values of θ are denser for larger z compared with the calculation as seen from Fig. 14, and for droplets of 250~350μ, the tendency becomes stronger. This arises probably from a fact that these droplets are ejected to some height when they are produced by disintegration of the jets. The ejection is most conspicuous for droplets of 300μ, as stated in **4.1.** If one considers that the origin of z-axis must be taken at some level above water surface owing to the ejection, for example, at $z=3$ cm for droplets of 100~150μ, at $z=6$ cm for those of 150~250μ and at $z=7$ cm for those of 250~300μ, the reduction factor takes values similar to the case of droplets smaller than 100μ. In Table 4, the reduction factor for droplets larger than 100μ is assumed to be 0.30. The calculated values in Fig. 14 are given after multiplied by the reduction factor. This sufficient consistency between the observation and the calculation confirms that droplets observed in the air above wind waves have been produced by bursting of air bubbles entrained in the way already described.

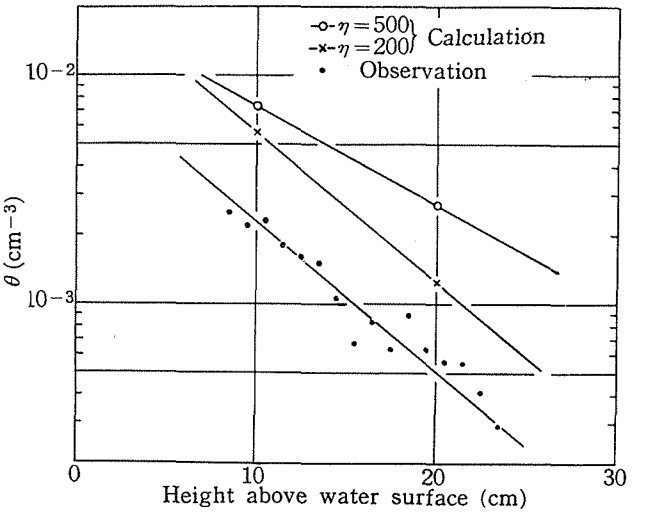

Fig. 15. Comparison among the distributions of θ calculated by assuming $\eta=500$ and $\eta=250$, and observed, for droplet diameter=50~100 μ, $\overline{W}=12.1\,\mathrm{m\cdot sec^{-1}}$ and fetch=13.6 m (see the context).

Table 4. Values concerning the droplets produced from wind waves when the wind speed is $22.8\,\mathrm{m\cdot sec^{-1}}$ (at 10 m level) (see the context).

I Drop diameter of center of size band (μ)	II Range of each size band (μ)	III w ($\mathrm{cm\cdot sec^{-1}}$)	IV F_1 for size band of II ($\mathrm{cm^{-2}\cdot sec^{-1}}$)	V F_1' for size band of II ($\mathrm{cm^{-2}\cdot sec^{-1}}$)	VI $\frac{F_1}{F_1'}$	VII $\frac{w\theta_0(x=13.6\,\mathrm{m})}{F_1}$	VIII F_1 for 10μ size band ($\mathrm{cm^{-2}\cdot sec^{-1}}$)	IX $F_1/w=\theta_0(x=\infty)$ for 10μ size band ($\mathrm{cm^{-3}}$)
8.6	< 13	0.22	0.11	—	—	0.012	0.13	0.58
17	13~ 22	0.85	0.161	—	—	0.044	0.19	0.22
26	22~ 30	2.0	0.147	—	—	0.10	0.17	0.086
34	30~ 39	3.5	0.078	—	—	0.17	0.091	0.026
43	39~ 47	5.4	0.035	—	—	0.26	0.041	0.0075
Sum			0.54	1.9	0.28			
60	47~ 73	10.2	0.125	—	—	0.44	0.048	0.0047
86	73~100	19.3	0.086	—	—	0.70	0.033	0.0017
Sum			0.21	0.71	0.30			
125	100~150	36.1	0.12	0.40	(0.30)	0.93	0.023	0.00064
200	150~250	68.8	0.12	0.39	(0.30)	0.95	0.012	0.00017
300	250~350	114	0.060	0.20	(0.30)		0.0060	0.000053

It must be noted here that the calculated values of θ lie nearly on straight lines in the graphs, together with points by observation. This shows that, although observed distribution of droplets appears exponential, it does not mean that the equilibrium condition expressed by Eq. (4) is obtained. In reality, the ratio $w\theta_0(x=13.6\,\mathrm{m})/F_1$, namely, the ratio of the rate of fall of droplets and the rate of production of them at 13.6 m in fetch, is calculated, and listed in column VII of Table 4, which shows that the smaller the droplets are, the farther the state is from the equilibrium, and that the equilibrium conditions (4) nearly hold only for droplets larger than 150μ. The distribution of θ calculated by Eq. (4) for 150~250μ in diameter is shown by a broken line in the figure. For 250~350μ in diameter, the calculation by Eq. (4) only is performed.

The obtained values of F_1 are converted respectively to the value for 10μ band of the droplet size, and are listed in column VIII of Table 4, and are shown in Fig. 16. The figure shows an outstanding peak at about 20μ in diameter. Also, it exhibits that a group of droplets produced through the shuttering of bubble

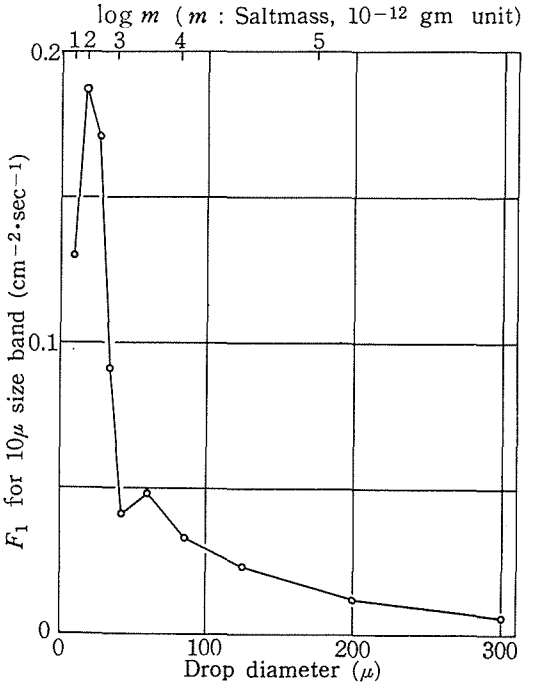

Fig. 16. Production rate of droplets from wind waves (F_1) when the wind speed is 22.8 m·sec^{-1} (at 10 m level). Values are shown for each 10μ size band of droplets.

film and which have diameters of a few tens μ, is superposed on a group of droplets which are produced through the jet disintegration and which seem to have a maximum frequency at about 60μ in droplet diameter.

It must be noted that, according to an estimation of the rate of evaporation of droplets in the wind flume before caught by the glass slides, droplets of the 8.6μ class may have been subjected to a significant change in size, so that a possibility arises that the degree of fall in the number of droplets, smaller than 20μ, is overestimated. However, this error belongs only to droplets smaller than 10^{-10} gm in the salt content, probably.

5.3. Distribution of sea-salt particles in the atmosphere

The value of F increases nearly linearly with the fetch, within short fetches as used in the experiment, and the value of F in equilibrium state cannot be estimated from the result of this experiment alone. But it may be supposed that it would not assume a value much different from F_1 (value of F at 13.6 m in fetch), because a value of wind stress over the water surface, measured at fetches

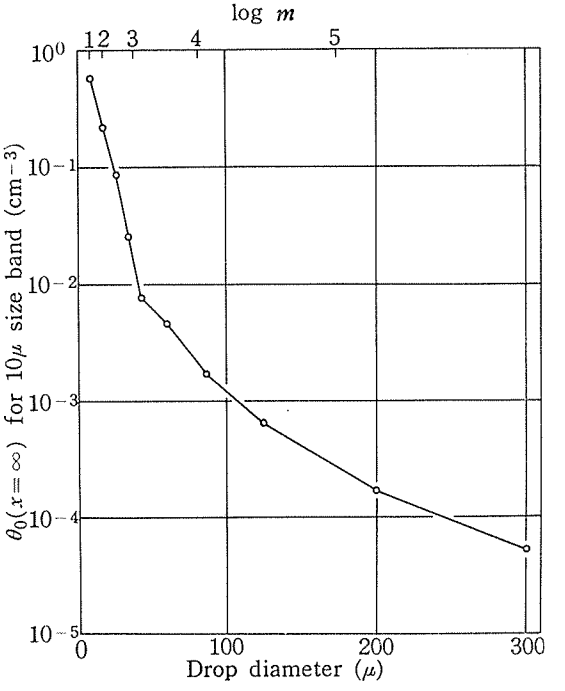

Fig. 17. Concentration of droplets at the surface of the open ocean (θ_0) when the wind speed is 22.8 m·sec^{-1} (at 10 m level). Values are shown for each 10μ size band of droplets.

greater than 10 m by use of the same wind flume by H. Kunishi (27), agrees with a value obtained by K. Brocks (28) at the North and Baltic Seas, and the value of α in **3.3** is also saturated already if the fetch exceeds 10 m. So, it is assumed that F is also saturated shortly and the value of F_1 nearly holds in the open ocean. This assumption will be ensured, in this and the next sections, by comparison of theoretical calculations using F_1 with actual observations.

The concentration of droplets at the surface of the open ocean is given by $\theta_0(x=\infty)=F_1/w$. The values of θ_0 calculated for 10μ size band are shown in column IX of Table 4 and in Fig. 17 for wind speed of 22.8 m·sec^{-1} (10 m level). From the figure, it is found that the concentration of droplets increases monotonously with a decreasing drop size, although the rate of production is maximum at 20μ diameter.

The size of droplets can be expressed by the mass of salt contained (m, in 10^{-12} gm unit) by assuming that the droplets consist of sea water. Fig. 17 has been redrawn in Fig. 18 by plotting $d\Theta_0/d(\log m)$ against $\log m$, where Θ_0 is the cumulative number of droplets, per unit volume of air at $z=0$ level, containing

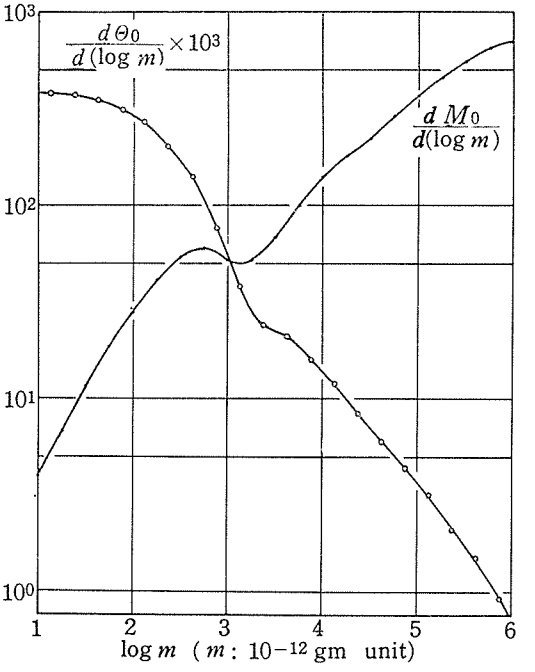

Fig. 18. Concentration-salt mass distribution and density-salt mass distribution of sea water droplets at the surface of the open ocean when the wind speed is 22.8 m·sec^{-1} (at 10 m level) (see the context).

salt less than or equal to m. The salt mass density M is defined as the total mass of sea salt, per unit volume of air, in droplets containing salt less than or equal to m, and the salt mass density-salt mass distribution at $z=0$ level is illustrated also in Fig. 18.

For the open ocean, Eq. (4) holds. Then comes

$$\log \frac{\theta_0}{\theta} = \frac{1}{2.3} \frac{w}{\eta} z ,$$

so that it is considered that for every distance of

$$\Delta z = 2.3 \eta / w ,$$

θ reduces to one order smaller. This distance is a function of w as well as of η, namely, it shows that larger droplets diminish rapidly at higher levels. Using this relation, one can estimate the salt mass density in the upper air from that at the sea surface. Using the values of terminal velocity of sea water droplets (w) shown in column III of Table 4, the salt mass density has been calculated for $z/\eta=0.1$, 1 and 2, and is illustrated in Fig. 19 by full lines. However, droplets do not remain as sea water droplets, but evaporate and become lighter, and the terminal velocity becomes smaller. The effect makes peaks of curves shift to

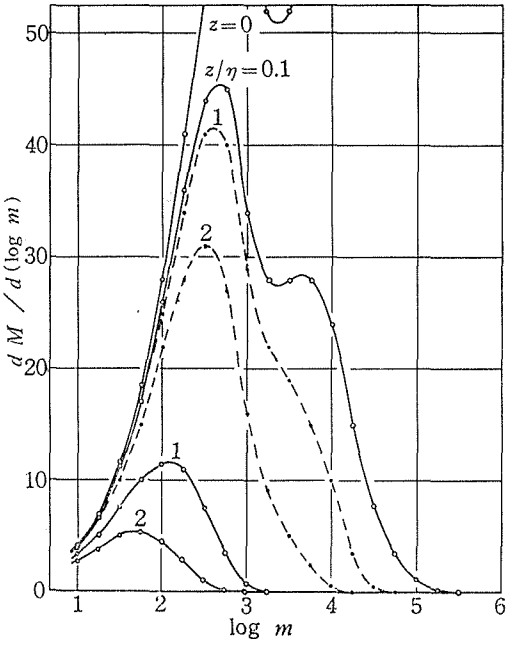

Fig. 19. Density-mass distribution of sea-salt particles at different heights (see the context).

the right. Using the values of w for dry sea-salt particles, the salt mass density has been calculated in the same way, and is illustrated by broken lines in Fig. 19. Actual conditions may lie between these two cases.

The salt mass density has a maximum value at $\log m=6$ for $z=0$, as seen from Fig. 18, but it has at about $\log m=3$ for $z/\eta=0.1$, and at around $\log m=2$ for $z/\eta=1$ or 2. If one assumes η in the lower atmosphere to be 10^4, $z/\eta=0.1$ will correspond to the condition at 10 m level, and $z/\eta=1$ at 100 m level. If η is 10^5, $z/\eta=1$ will correspond to the condition at 1000 m level. E. Eriksson (**29**) calculated the density-mass distribution from flight observations by A. H. Woodcock (**30, 31**) of sea-salt nuclei in the atmosphere at different wind forces, and obtained curves having similar features to those in Fig. 19. Considering that Fig. 19 represents a case of wind force=9, one may find that the order of magnitude is compatible with each other. The distribution of θ in the atmosphere is a complicated problem in meteorology, nevertheless the above fact seems to give a good support to the assumption that the values of F_1 represent the production rate of sea-water droplets at the open ocean surface for wind force=9. The other support will be given in the following section.

As to the position of the maxima of the curves in Fig. 19, one find that they shift to the left compared to Eriksson's figure. This may be explained by the coalescence of droplets in the course of their circulation.

5.4. Salt fallout near the coast, and dependence on wind speed

I. Kita and T. Aya (**32**) measured the rate of fallout of sea salt, between 20 m and 1000 m inland from the coast of Tadotsu, under a condition of the wind speed up to 20 m·sec^{-1}, and obtained the following empirical law:

$$q = e^{0.34u+0.8}x^{-1}, \qquad (7)$$

where q represents the rate of fallout of Cl in mg·m^{-2}·hr^{-1}, u the wind velocity in m·sec^{-1}, and x the distance from the coast line in m. If one assumes that the salt fallout has the same contents with sea water and considers the rate of fallout of total sea salt, q', in 10^{-6} mg·cm^{-2}·sec^{-1}, the above formula will be reduced to

$$q' = e^{0.34u-2.19}x^{-1}. \qquad (8)$$

The formula (8) is calculated for $u=22.8$, and the value is shown by a broken line in Fig. 20.

On the other hand, using Eq. (6), the salt fallout on land near the coast can be calculated as follows:

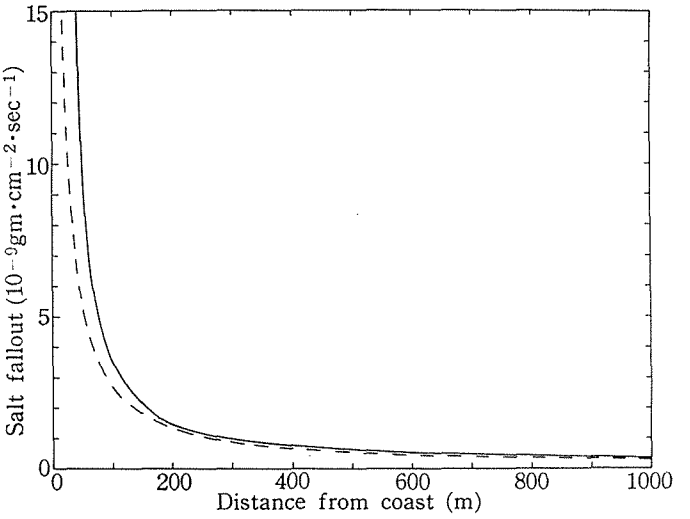

Fig. 20. Salt fallout near the coast. The full line is calculated by Eq. (6) by use of the value F_1, and the broken line represents the formula by KITA and AYA (32) (see the context).

$$q'(x,u) = \sum m w \theta_0$$
$$= \sum m F w \left[\frac{1}{w} - \int_0^x \left\{\frac{1}{\sqrt{\pi\eta u x}} e^{-\frac{w^2 x}{4\eta u}} - \frac{w}{2\eta u}\operatorname{erfc}\left(\frac{w\sqrt{x}}{2\sqrt{\eta u}}\right)\right\} dx\right], \qquad (9)$$

where the summation must be performed concerning the droplet size grade. Eq. (9) is calculated by using the value of F_1 in column IV in Table 4. An example of the calculation of θ_0, by using values $\eta = 5\times10^3$ and $u = 2\times10^3$ (c.g.s. units), which are the conditions at about 2 m level for wind speed of 22.8 m·sec^{-1}, is shown in Fig. 21. The calculated value of q' is shown by a full line in Fig. 20.

If the full line is translated to the left by 25 m, it agrees with the broken line exactly. This means that $x=0$ has been taken at 25 m off-shore in the calculation. In reality, there is a sea-bank about 3 m high, and it is considered that droplets produced near the sea-bank are not brought on land. The retreat of 25 m of $x=0$ line in the calculation, therefore, would not be unreasonable. The above best agreement seems to ensure the validity of the value of F_1 used as the value at the open ocean.

In the empirical law due to Kita and Aya, the wind factor is expressed by $\exp(0.34u)$, when u is measured in m·sec^{-1}. On the other hand, as seen from Eq. (9), the rate of salt fallout on land is proportional to the value of F, as far as a

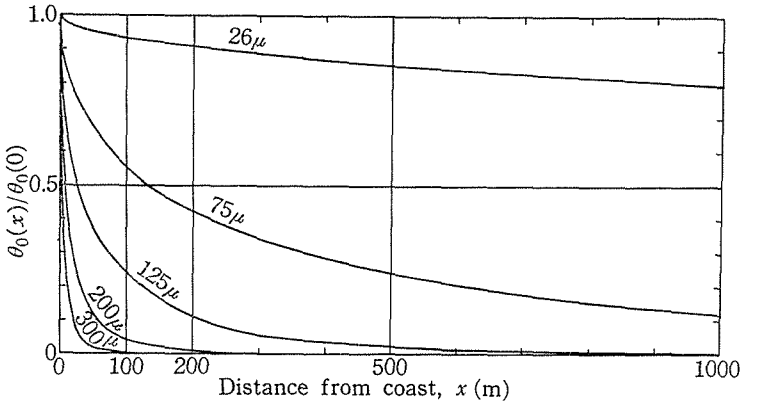

Fig. 21. Ratio $\theta_0(x)/\theta_0(0)$ calculated by Eq. (6) for five grades of droplet diameter.

class of droplets of the same size is concerned. Now, values of F_1' in Table 3 are multiplied by the reduction factor of 0.3 owing to bubble flocking, and the change of the rate of salt production with wind speed is obtained for the three classes of droplet size smaller than 150μ, because classes of larger droplets do not contribute to the salt fallout farther than several tens of the meter from the coast, as Fig. 21 shows. The values also depend on the wind speed exponentially and F or mF can be expressed roughly by the relation:

$$F \text{ or } mF = e^{0.40u+\text{const.}} \qquad (u : \text{m}\cdot\text{sec}^{-1}) , \tag{10}$$

in the range of the wind speed between 15 m·sec^{-1} and 23 m·sec^{-1}. Thus, the wind factor given by Eq. (10) agrees well with the result of field observation.

5.5. Coefficient of mixing in wind waves

In wind waves, there is scarcely any net transport of bubbles in the x-direction, so that the distribution of bubble concentration can be expressed by the equation

$$w\frac{\partial\theta}{\partial z}+\eta\frac{\partial^2\theta}{\partial z^2}=0 , \tag{11}$$

where θ represents the concentration of bubble in water, w the terminal velocity of bubbles rising through water, η the coefficient of mixing in wind waves, and the z-axis is taken positive downward from the water surface. The boundary conditions in this case are

$$\left.\begin{aligned} &\theta = 0 \qquad \text{at} \quad z=\infty , \\ \text{and} \quad &\frac{\partial\theta}{\partial z}=-\frac{B}{\eta} \qquad \text{at} \quad z=0 , \end{aligned}\right\} \tag{12}$$

where B is the time rate of the bubble formation at the water surface per unit area. If η=const., the solution is

$$\theta = \frac{B}{w} e^{-\frac{w}{\eta}z} = \theta_0 e^{-\frac{w}{\eta}z}, \tag{13}$$

and θ decreases exponentially with z.

As the average distribution of bubble concentration decreases nearly exponentially with depth, as shown in **3.2**, it is considered that the above condition holds in the range of the depth where bubbles are entrained, and one can estimate the value of η from the gradient of the graph showing the observed distribution of θ, namely,

$$\eta = \frac{wz}{2.3(\log \theta_0 - \log \theta)}. \tag{14}$$

Now, for the three examples shown in **3.2**, the value of η is calculated for each grade of the bubble diameter. They are shown in Table 5, together

Table 5. Coefficient of mixing in wind waves, estimated from vertical distribution of the entrained air bubbles.

Bubble diameter of center of size band (mm)		0.25	0.75	1.25	1.75	2.25	2.75	3.0<	(From the total number of bubbles)
w (cm·sec^{-1})		4.0	12	20	28	29	27	25	(20)
η(cm^2·sec^{-1})	$\overline{W}$=12.1 m·sec^{-1} Fetch=13.6 m	14	54	60	78	97	66	47	56
	$\overline{W}$=12.1 m·sec^{-1} Fetch=10.0 m	9	35		29	31		26	43
	$\overline{W}$=11.6 m·sec^{-1} Fetch=13.6 m	16	48	74	75	71	80	66	60

with the value of w used in the calculation. From this, it appears that the estimated values of η increase with the values of w, and the relation between η and w is given by

$$\eta = 6.5\, w^{3/4} \qquad \text{(c.g.s.)},$$

that is, $z/[2.3(\log \theta_0 - \log \theta)]$ is proportional to $w^{-1/4}$. The apparent change of η with w may be attributed to the change of w itself due to an interaction among many bubbles rising through water, because the values of w used in the above calculation are based on the data for single bubbles given by R. L. Datta *et al.* (**21**). If the value of η is assumed to be constant for all w as in the above reduction, though it is probably a function of z, the constant value of η will be obtained by assuming the actual rising velocity of bubbles (w') to be

$$w' = Cw^{1/4}, \tag{15}$$

where C is a constant. Eq. (15) means that the rising velocity of bubbles is somewhat averaged in the case of grouping. Using this w' instead of w in Eq. (14), one obtains

$$\eta = 6.5\,C\,.$$

The value of C cannot be determined unless the independent estimation of η or w' is carried out. The values of η obtained from the distribution of total bubble concentration shown in **3.2** (Fig. 9) by use of a provisional representative value of $w=20\,\mathrm{cm\cdot sec^{-1}}$, are tabulated in the right column of Table 5.

6. Concluding remarks

From the above studies we may come to the following conclusion. When the wind speed exceeds about $13\,\mathrm{m\cdot sec^{-1}}$ (10 m level), small wavelets in which the surface tension exerts to a considerable degree and which have a profile that peaks downward, begin to enclose air bubbles at their troughs on crests of underlying gravity waves. The bubbles produce small droplets when they burst at the sea surface. Splashing water from wave crests is in large drops which fall back quickly into the sea, but droplets which are produced from bubbles and which contain salt less than $10^{-7}\sim10^{-8}\,\mathrm{gm}$ are easily transported into the upper air by atmospheric turbulence, and form atmospheric condensation nuclei, among which the giant sea-salt nuclei can initiate rain from warm clouds. These smaller sea-salt particles are transported, as far as the inner part of continents, ceaselessly and play an important role in the circulation of materials on the earth. Comparatively large droplets are also transported as far as several hundred meters from the coast, and cause salt spray damage of the coastal plant.

There are at least two different mechanisms for droplet production by bursting bubbles, and they belong to either of the two bubble size ranges which are divided by a few mm in diameter. Droplets carried up into the upper air or transported far inland are produced mostly by film shuttering of bubbles of several mm. This is derived from bubble size distribution in wind waves, the number of droplets produced from each bubble, and the diffusivity of droplets in the atmosphere.

As to the dependence of the rate of droplet production on wind speed u ($\mathrm{m\cdot sec^{-1}}$ at 10 m level), it is expressed approximately by $\exp(0.40u)$ in the range of the wind speed between $15\,\mathrm{m\cdot sec^{-1}}$ and $23\,\mathrm{m\cdot sec^{-1}}$. The rate of production of droplets of each size grade for the wind speed of $23\,\mathrm{m\cdot sec^{-1}}$, is shown in Fig. 16 and column IV in Table 4. For this wind speed, the rate of production of sea-water droplets having diameter from several to 150μ (containing $10^{-11}\,\mathrm{gm}\sim8\times10^{-8}\,\mathrm{gm}$ of sea-salt), amounts to $0.87\,\mathrm{cm^{-2}\cdot sec^{-1}}$ in number, and to

6.0×10^{-9} gm·cm^{-2}·sec^{-1} in total mass of salt. If one considers droplets from several to 100μ (from 10^{-11} gm to 3×10^{-8} gm in sea-salt), the values become 0.75 cm^{-2}·sec^{-1} and 1.7×10^{-9} gm·cm^{-2}·sec^{-1}, respectively.

The above estimated production rate of sea-water droplets has been checked, by connecting it theoretically with actual data of giant sea-salt nuclei obtained by A. H. Woodcock, and with data of salt fallout near the coast. Now, the rate of salt production may also be considered as a link of sea-salt circulation on the earth. E. Eriksson (**29**) estimated the rate of total sea-salt deposition over the oceans to be about 10^{-11} gm·cm^{-2}·sec^{-1}. On the other hand, the concentration of chloride in rain water has been measured by many investigators, and there is an outstanding tendency that it decreases nearly exponentially with distance from the coast. Generally, the concentration seems to be less than 20 mg·l^{-1} even at coastal areas (**33**). This corresponds to the yearly total deposition of chloride by precipitation of 200 kg·ha^{-1}·year^{-1} in maximum, for 1000 mm of annual precipitation. This value is seen also in figures by Eriksson (**29**). If the deposition rate of chloride (including dry deposition) over the oceans is twice this value, it will become 10^{-10} gm·cm^{-2}·sec^{-1}. Depositon of the sea-salt on the continents is, according to Eriksson (**29**), only about 10 per cent of the total deposition on the earth. Hence, if one assumes that droplets smaller than 100~150μ produced at the sea surface are all transported into the upper air, one will come to a conclusion that atmospheric sea-salt is sufficiently furnished if only from a few per mille to a few per cent of sea surface area is always exposed to the wind of 23 m·sec^{-1}. On the other hand, B. J. Mason (**34**) states that if the sea surface is to be capable of supplying enough condensation nuclei for cloud formation, it must produce them at a rate of about 10^4·m^{-2}·sec^{-1} in number in the regions where waves are breaking. Even if only one tenth of the atmospheric condensation nuclei is sea-salt, the above rate will be 10^3·cm^{-2}·sec^{-1}. The result of the present study has revealed that the rate of droplet and bubble formation is 0.8 cm^{-2}·sec^{-1} for 23 m·sec^{-1} in wind speed. If one bubble produces 100~200 droplets of the third group that contain salt of 10^{-14}~10^{-15} gm as stated in **4.1**, the production rate will become only of the order of 10^2. Thus the rate of production of atmospheric sea-salt is sufficient in amount, but deficient in number. This conclusion seems to suggest that one droplet produces many minute secondary salt nuclei while it stays in the air and evaporates (**35**, **36**, **37**, **38**, **39**, **40**), although giant sea-salt nuclei may coalesce one another as shown in **5.3**.

Acknowledgements

The author wishes to express his sincere gratitude to Prof. Shōitirō Hayami for his cordial guidance and encouragement throughout this study. He thanks

to Assis. Prof. Hideaki Kunishi for numerous advices. He also thanks to Mr. Haruo Higuchi and other members of the Ujigawa Hydraulics Laboratory of Disaster Prevention Research Institute, Kyoto University, who provided facilities in carrying out the present experiment.

REFERENCES

1. S. G. Boyce, The salt spray community, Ecological Monogr., **24** (1954), 29.
2. A. H. Woodcock, C. F. Kientzler, A. B. Arons and D. C. Blanchard, Giant condensation nuclei from bursting bubbles, Nature, **172** (1953), 1145.
3. C. F. Kientzler, A. B. Arons, D. C. Blanchard and A. H. Woodcock, Photographic investigation of the projection of droplets by bubbles bursting at a water surface, Tellus, **6** (1954), 1.
4. F. Knelman, N. Dombrowski and D. M. Newitt, Mechanism of the bursting of bubbles, Nature, **173** (1954), 261.
5. D. J. Moore and B. J. Mason, The concentration, size distribution and production rate of large salt nuclei over the oceans, Quart. J. Roy. Meteor. Soc., **80** (1954), 583.
6. B. J. Mason, Bursting of air bubbles at the surface of sea water, Nature, **174** (1955), 470.
7. D. C. Blanchard and A. H. Woodcock, Bubble formation and modification in the sea and its meteorological significance, Tellus, **9** (1957), 145.
8. S. Hayami and Y. Toba, Drop production by bursting of air bubbles on the sea surface (I). Experiments at still sea water surface, J. Oceanogr. Soc. Japan, **14** (1958), 145.
9. K. Isono, Microphysical processes in precipitation mechanism, Japanese J. Geophys., **2** (1959), 1.
10. H. Kunishi, On design of resistive wave meter, Dis. Prev. Res. Inst. Annuals, **3** (1959), 65.
11. Y. Toba, Observation of sea water droplets by filter paper, J. Oceanogr. Soc. Japan, **14** (1958), 151.
12. K. R. May, Apparatus for coating surfaces with magnesium oxide, J. Sci. Instr., **17** (1940), 231.
13. K. R. May, The cascade impactor. An instrument for sampling coarse aerosols, J. Sci. Instr., **22** (1945), 187.
14. K. R. May, The measurement of airborne droplets by the magnesium oxide method, J. Sci. Instr., **27** (1950), 128.
15. A. H. Woodcock and M. M. Gifford, Sampling atmospheric sea-salt nuclei over the ocean, J. Marine Res., **8** (1949), 177.
16. W. H. Munk, High frequency spectrum of ocean waves, J. Marine Res., **14** (1955), 302.
17. A. H. Schooley, Profiles of wind-created water waves in the capillary-gravity transition region, J. Marine Res., **16** (1958), 100.
18. P. J. H. Unna, White horses, Natare, **148** (1941), 226.
19. W. H. Munk, A critical wind speed for air-sea boundary processes, J. Marine Res., **6** (1946), 203.
20. G. D. Crapper, An exact solution for progressive capillary waves of arbitrary amplitude, J. Fluid Mech., **2** (1957), 532.
21. R. L. Datta, D. H. Napier and D. M. Newitt, The properties and behaviour of gas bubbles formed at a circular orifice, Trans. Instn Chem. Engrs., **28** (1950), 14.
22. O. Stuhlman, Jr., The mechanics of effervescence, Physics, **2** (1932), 457.
23. D. M. Newitt, N. Dombrowski and F. H. Knelman, Liquid entrainment I. The mechanism of drop formation from gas or vapour bubbles, Trans. Instn Chem. Engrs., **32** (1954), 244.
24. Y. Toba, Drop production by bursting of air bubbles on the sea surface (II). Theoretical study on the shape of floating bubbles, J. Oceanogr. Soc. Japan, **15** (1959), 121.

25. S. OKUDA and S. HAYAMI, Experiments on evaporation from wavy water surface, Rec. Oceanogr. Works Japan, **5** (New series) (1959), 6.
26. W. R. LANE and H. L. GREEN, The mechanics of drops and bubbles in *Surveys in Mechanics* (Cambridge University Press, 1956), 162.
27. H. KUNISHI, Unpublished paper.
28. K. BROCKS, Measurements of wind profiles over the sea and the drag at the sea surface, International Oceanographic Congress, Preprints (1959), 742.
29. E. ERIKSSON, The yearly circulation of chloride and sulfur in nature; meteorological and pedological implications, Tellus, **11** (1959), 375; **12** (1960), 63.
30. A. H. WOODCOCK, Salt nuclei in marine air as a function of altitude and wind force, J. Meteor., **10** (1953), 362.
31. A. H. WOODCOCK, Atmospheric sea-salt nuclei data for Project Shower, Tellus, **9** (1957), 521.
32. I. KITA and T. AYA, Observation of the scattering of saline drops near the seashore inland by strong wind. J. Meteor. Res., **11** (1959), 373 (in Japanese).
33. E. ERIKSSON, Composition of atmospheric precipitation, Tellus **4** (1952), 215; 280.
34. B. J. MASON, *The Physics of Clouds* (Clarendon Press, Oxford, 1957).
35. H. DESSENS, Les noyaux de condensation de l'atmosphére, C. R. Acad. Sci., **223** (1946), 915.
36. Y. MIYAKE, The chemical nature of the saline matter in the atmosphere, Geophys. Mag., **16** (1948), 64.
37. K. SUGAWARA, S. OANA and T. KOYAMA, Separation of the components of atmospheric salt and their distribution, Bull. Chem. Soc. Japan, **22** (1949), 47.
38. T. KOYAMA and K. SUGAWARA, Separation of the components of atmospheric salt and their distribution (continued), Bull. Chem. Soc. Japan, **26** (1953), 123.
39. W. E. RANZ and W. R. MARSHALL, Evaporation from drops, Chem. Engr. Prog., **48** (1952), 141; 173.
40. S. TWOMEY and K. N. MCMASTER, The production of condensation nuclei by crystallizing salt particles, Tellus, **7** (1955), 458.